A Robust Scheme for TD-MoM Analysis of Planar PEC Objects

A. Soltani [1], Z. H. Firouzeh [1], and H. R. Karami [2]

[1] Department of Electrical and Computer Engineering
Isfahan University of Technology, Isfahan, 8415683111, Iran
afsun.soltani@ec.iut.ac.ir, zhfirouzeh@gmail.com

[2] Department of Electrical Engineering
Bu-Ali Sina University, Hamedan, 65178, Iran
hamidr.karami@basu.ac.ir

Abstract ─ A robust, fast and simple scheme for calculation of potential integrals that encountered singular terms in time domain integral equation (TDIE) for planar PEC scatterers in free space is presented. In this method singular terms of the potential integrals, like other terms, calculated numerically by selecting some points in the source and observation patches in TD-MoM solver. In fact this method cancelled dealing with the singularity of self-terms.

The numerical integration of the potential integrals is almost two times faster than other methods that extracted or cancelled singularity of self-terms. Numerical results illustrate the accuracy and simulation time of the proposed technique.

Index Terms ─ Potential integral, singularity, time domain and numerical integration.

I. INTRODUCTION

Perfect electric conductor (PEC) surfaces in electromagnetic structures are used in many applications such as electromagnetic interference (EMI), electronic packaging, radar cross section, and antenna design [1, 2]. Numerical techniques for the prediction of electromagnetic fields scattered by complex objects, directly operating in time domain (TD), have recently received considerable attention [3].

Time domain analysis of PEC surfaces is required due to using narrow band exciting pulse to obtain the transient response in initial moments in some cases. Numerically solutions for this analysis are usually based on surface integral equation (IE) formulations [4]. To solve the time-domain integral equations, method of moments (MoM) [5] is selected as the most common numerical method. In the MoM solution, the induced electric and magnetic currents are unknowns, and the surface of the scatterers or targets is usually subdivided into small planar patches of a simple shape [6]. These unknown currents approximated by the basis functions. Depending on the shape of patches, the suitable basis function is selected.

In the process of MoM, we deal with evaluation of double integrals with singular kernels of surface integral equation (IEs) [6]. These singular kernels related to the potential integrals in the IEs of electromagnetics need to be evaluated analytically or numerically. Singularities occur when testing and source subdomains coincide in the kernels of self-terms in the MoM procedure [7].

Several singularity subtraction or cancellation methods have been proposed. For example, analytic and numerical integration are proposed by Gibson [1], a new singularity subtraction integral formula [6], Duffy's transformation [8], Khayat-Wilton method [7], analytical evaluation method [9], analytical computation of singular part [10], an accurate method for the calculation of singular integrals [11] and a proposed method in [12] for the evaluation of singular integrals arising in method of moments. Almost all the methods suffer from a few disadvantages; for instance, Duffy's transformation is derived for functions having a point singularity of order 1/R so singularities of order $\nabla(1/R)$ appeared in integral equations cannot be easily evaluated [13]. Also, Duffy's transformation does not work well for nearly singular integrals occurring when an observation point is near a source point [3]. For the method presented in [6], a new subtraction method is introduced that covers both triangular and rectangular basis functions but the singularity subtraction is based on Taylor's series at R=0 in which R is the distance between testing and source subdomains. Therefore, it is valid only for sufficiently small values of R and the accuracy of the computation is deteriorated for large values of R [6]. In another research [12], the kernels of integrals arising in method of moments are categorized to regular, nearly singular, weakly singular and strongly singular. For each of these different types of integrals, a particular method is presented leading to complicated calculation procedure. Other mentioned methods also suffer from complexity

Submitted On: October 28, 2016
Accepted On: January 28, 2017

analytical computation of singular terms in regard to the other terms.

In this paper, we analyse the time-domain mixed potential integral equation (TD-MPIE) of PEC surfaces in free space with calculation of the potential integrals by a simple method that does not deal with extracting or cancelling the singularity of self-terms. In fact, a few points are used for source and observation patches resulting in the calculation of the potential integrals numerically. The proposed method based on Makarov's work [14] is extended for multi-points in source and observation patches in time domain. This method is compared with analytic and numerical integration proposed by Gibson [1] since the Gibson method has used analytical singularity calculation regarding to the other introduced methods. The Gibson method can be applied to N-sided planar polygons of an arbitrary shape. Also, its singularity computation is independent on the type of integral equation formulation. Also the Gibson method is accurate enough to compare with the other methods.

II. FORMULATION

Let *S* denote the surface of a finite PEC in free space illuminated by a transient electromagnetic pulse as shown in Fig. 1. This pulse induces a surface current, $\boldsymbol{J}(\boldsymbol{r}, t)$, on *S* which then reradiates a scattered field.

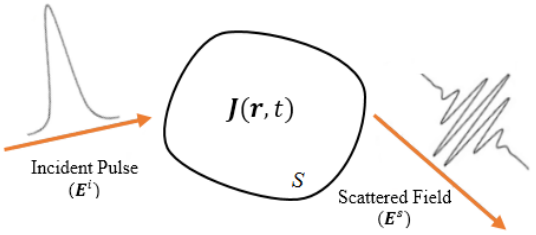

Fig. 1. A PEC excited by incident electromagnetic field.

The boundary conditions require that the total tangential electric field on PEC be zero or,

$$\{\boldsymbol{E}^s + \boldsymbol{E}^i\}_{tan} = 0. \quad (1)$$

The scattered fields radiated by the current $\boldsymbol{J}(\boldsymbol{r}, t)$, may be written in terms of the magnetic vector $\boldsymbol{A}(\boldsymbol{r}, t)$ and electric scalar potentials $\Phi(\boldsymbol{r}, t)$ as [15]:

$$\boldsymbol{E}^s = -\frac{\partial \boldsymbol{A}}{\partial t} - \nabla\Phi, \quad (2)$$

where

$$\boldsymbol{A}(\boldsymbol{r}, t) = \mu \int \frac{\boldsymbol{J}(\boldsymbol{r}', t - R/c)}{4\pi R} ds', \quad (3)$$

and

$$\Phi(\boldsymbol{r}, t) = \frac{1}{\epsilon} \int \frac{q_s(\boldsymbol{r}', t - R/c)}{4\pi R} ds', \quad (4)$$

and $R = |\boldsymbol{r} - \boldsymbol{r}'|$. In Equations (1)-(4), μ and ϵ are the permeability and permittivity of the surrounding medium, *c* is the velocity of propagation of the electromagnetic wave, and $\boldsymbol{r}$ and $\boldsymbol{r}'$ are the arbitrarily located observation point and source point on the scatterer, respectively.

Surface charge density q_s in Equation (4) is related to the surface divergence of $\boldsymbol{J}$ through the continuity equation, so the scalar potential term can be given as:

$$\Phi(\boldsymbol{r}, t) = -\frac{1}{4\pi\epsilon} \int \int_0^{t - R/c} \frac{\nabla_s \cdot \boldsymbol{J}(\boldsymbol{r}', \tau)}{R} d\tau ds'. \quad (5)$$

Using Equation (1) and Equation (2), the time domain electric field integral equation (TD-EFIE) can be obtained as follows:

$$\left\{\frac{\partial \boldsymbol{A}(\boldsymbol{r}, t)}{\partial t} + \nabla\Phi(\boldsymbol{r}, t)\right\}_{tan} = \boldsymbol{E}^i_{tan}(\boldsymbol{r}, t). \quad (6)$$

For the numerical solution of Equation (6), we now approximate the conducting surface by triangular patches and employ the triangular current expansion on *S* by:

$$\boldsymbol{J}(\boldsymbol{r}, t) = \sum_{k=1}^{N} I_k(t) \boldsymbol{f}_k(\boldsymbol{r}). \quad (7)$$

N is the number of non-boundary edges. Note that a boundary edge is an edge which is associated with only one triangular patch. $I_k(t)$ represents a temporal basis function and $\boldsymbol{f}_k(\boldsymbol{r})$ is the vector basis function associated with the *k*th edge. As in [16], the vector basis function is defined as:

$$\boldsymbol{f}_k(\boldsymbol{r}) = \begin{cases} \frac{l_k}{2A_k^{\pm}} \boldsymbol{\rho}_k^{\pm} & \boldsymbol{r} \in T_k^{\pm} \\ 0 & otherwise \end{cases}, \quad (8)$$

where l_k and $A_k^{\pm}$ are the length of the edge and the area of the triangle $T_k^{\pm}$, respectively and $\rho_k^{\pm}$ are the position vectors referenced at the free vertex of $T_k^{\pm}$, as shown in Fig. 2. The surface divergence is then given by:

$$\nabla . \boldsymbol{f}_k(\boldsymbol{r}) = \begin{cases} \frac{l_k}{A_k^+} & \boldsymbol{r} \in T_k^+ \\ -\frac{l_k}{A_k^-} & \boldsymbol{r} \in T_k^- \\ 0 & otherwise \end{cases}. \quad (9)$$

Using time domain MoM (TD-MoM) solver for the TD-MPIE and Galerkin method, the spatial test functions are the same as the expansion function $\boldsymbol{f}_k(\boldsymbol{r})$. The inner product is chosen as:

$$\langle \boldsymbol{a}, \boldsymbol{b} \rangle = \int \boldsymbol{a} . \boldsymbol{b}\, ds. \quad (10)$$

We divide the times axis into equal intervals of segment Δt, and define $t_j = j\Delta t$. By applying the testing procedure to Equation (6), and approximating the time derivative by the forward-difference approximation, we can rewrite Equation (6) as:

$$\langle \boldsymbol{f}_k, \boldsymbol{A}(\boldsymbol{r}, t_j) \rangle + \langle \boldsymbol{f}_k, (\Delta t)\nabla_s \Phi(\boldsymbol{r}, t_j) \rangle = \langle \boldsymbol{f}_k, (\Delta t)\boldsymbol{E}^i(\boldsymbol{r}, t_j) \rangle + \langle \boldsymbol{f}_k, \boldsymbol{A}(\boldsymbol{r}, t_{j-1}) \rangle . \quad (11)$$

Next, using the vector identity $\nabla_s . (\Phi \boldsymbol{A}) = \boldsymbol{A} . \nabla_s \Phi + \Phi \nabla_s . \boldsymbol{A}$, and using the properties of the basis function [16], we rewrite Equation (11) as:

$$\langle \boldsymbol{f}_k, \boldsymbol{A}(\boldsymbol{r}, t_j) \rangle - \langle \nabla_s . \boldsymbol{f}_k, (\Delta t)\Phi(\boldsymbol{r}, t_j) \rangle = \langle \boldsymbol{f}_k, (\Delta t)\boldsymbol{E}^i(\boldsymbol{r}, t_j) \rangle + \langle \boldsymbol{f}_k, \boldsymbol{A}(\boldsymbol{r}, t_{j-1}) \rangle . \quad (12)$$

Thus, substituting Equation (3) and Equation (4) into Equation (12) yields, after a few steps of algebra, the following set of Equations [15], given by:

$$\sum_{k=1}^{N} Z_{mk}^{a}(t_j) + \Delta t \sum_{k=1}^{N} Z_{mk}^{b}(t_j) = F_m(t_j) + \sum_{k=1}^{N} Z_{mk}^{a}(t_{j-1}) \quad m = 1,2,\dots N, \tag{13}$$

where

$$Z_{mk}^{a}(t_j) = O_{mk}^{++} + O_{mk}^{\pm} + O_{mk}^{\mp} + O_{mk}^{--}, \tag{14}$$

$$Z_{mk}^{b}(t_j) = Q_{mk}^{++} - Q_{mk}^{\pm} - Q_{mk}^{\mp} + Q_{mk}^{--}, \tag{15}$$

$$O_{mk}^{\pm\pm} = \{I_k(t_R^{\pm\pm})\}\{\frac{\mu l_m l_k}{2A_k^{\pm}}\rho_m^{\pm}.\int_{T_k^{\pm}} \frac{\rho_k^{\pm}}{4\pi R_{mk}^{\pm\pm}} ds'\}, \tag{16}$$

$$Q_{mk}^{\pm\pm} = \left\{\int_0^{t_R^{\pm\pm}} I_k(\tau)d\tau\right\}\left\{\frac{l_m l_k}{\epsilon A_k^{\pm}}\int_{T_k^{\pm}} \frac{ds'}{4\pi R_{mk}^{\pm\pm}}\right\}, \tag{17}$$

and

$$F_m(t_j) = \frac{l_m \Delta t}{2}\{\rho_m^{c+}.\boldsymbol{E}^i(\boldsymbol{r}_m^{c+}, t_j) + \rho_m^{c-}.\boldsymbol{E}^i(\boldsymbol{r}_m^{c-}, t_j)\}. \tag{18}$$

In Equation (16) and Equation (17), $A_k^{\pm}$ represents the area of the triangle $T_k^{\pm}$, $t_R^{\pm\pm} = t_j - R_{mk}^{\pm\pm}/c$, and $R_{mk}^{\pm\pm}$ is the distance between the source and observation patches.

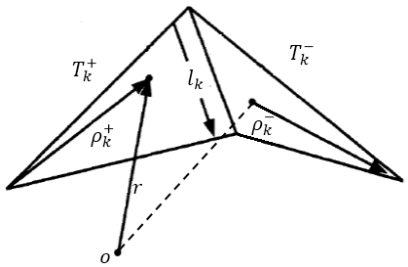

Fig. 2. The spatial vector basis function.

To calculate the distance between the source and observation patches, we consider special points in triangle patches corresponding to the source and observation as shown in Fig. 3 and Fig. 4, respectively. Actually, the distance between source and observation patches is the difference between two matrixes that the elements of each one contain the position of selected points. To clear the matter, if we select n points from p_1 to p_n in the source patch and m points from q_1 to q_m in the observation patch, the distance define as:

$$\boldsymbol{R} = \begin{bmatrix} x_{p1} & x_{p2} & \cdots & x_{pn} \\ y_{p1} & y_{p2} & \dots & y_{pn} \\ z_{p1} & z_{p2} & \dots & z_{pn} \end{bmatrix} - \begin{bmatrix} x_{q1} & x_{q2} & \cdots & x_{qm} \\ y_{q1} & y_{q2} & \dots & y_{qm} \\ z_{q1} & z_{q2} & \dots & z_{qm} \end{bmatrix}. \tag{19}$$

So we obtain:

$$\int_{T_m} \frac{1}{\boldsymbol{R}} = \frac{A_m}{F}\sum_{k=1}^{F} \frac{1}{|\boldsymbol{r}_s(k) - \boldsymbol{r}_o(k)|}. \tag{20}$$

A_m is the area of the triangle, F is the lowest common multiple of the number of source and observation points, and $\boldsymbol{r}_s$ and $\boldsymbol{r}_o$ are the position of source and observation points, respectively.

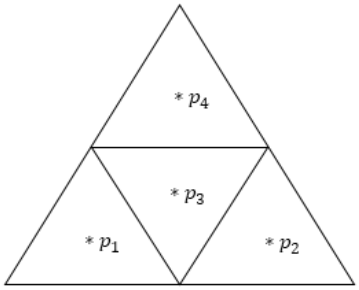

Fig. 3. Source patch barycenteric subdivision.

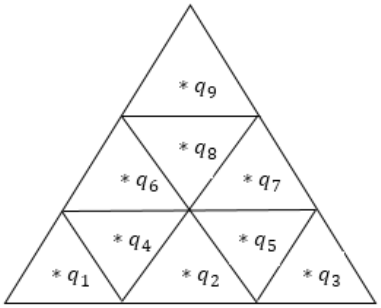

Fig. 4. Observation patch barycenteric subdivision.

III. NUMERICAL RESULTS

In this section, we present the numerical results of applying the presented method on various structures. Also, the results compared within the analytic and numerical method presented by Gibson [1] that calculates potential integrals with singular kernel of $1/R$. All the objects are illuminated by a Gaussian plane wave, given by:

$$\boldsymbol{E^i}(\boldsymbol{r}, t) = E_0 \frac{4}{\sqrt{\pi}T} e^{-\gamma^2}, \tag{21}$$

where

$$\gamma = \frac{4}{T}\{ct - ct_0 - \boldsymbol{r}\cdot\boldsymbol{a_k}\}, \tag{22}$$

with $E_0 = 120\pi \boldsymbol{a_x}, \boldsymbol{a_k} = -\boldsymbol{a_z}, T = 13.34\, ns,$ and $ct_0 = 20\, ns$.

First, to choose optimum number of points in source and observation patches, we consider a 1m × 1m square plate, located in the *xy* plane and centered about the origin. By changing the number of points, some that cause stable response have been listed in Table 1. For each case, the relative error, the exact value presented by Gibson [1] is used, and the computation time have been computed. We select 9 and 16 points for source and observation patches, respectively.

As shown in Table 1, as the number of selection points is greater, the relative error reduces but the

computation time increases. So, this choice of numbers is optimum. The following consideration has been done based on 9 and 16 points for source and observation patches, respectively.

The mentioned unit square PEC plate has been subdivided into 44 triangular patches with 58 unknowns. Figure 5 shows the space-time distribution of *x*-directed current induced at center of the square using the proposed solution and the results are compared with the Gibson method [1]. The curves show the good agreement between two methods. Also, the currents induced at the corners of the square are depicted in Fig. 6.

Table 1: Computation time and relative error for different source and observation points

No. of Source Points	No. of Observation Points	Computation Time (S)	Relative Error (%)
4	9	8.464983	0.0093
9	16	8.860424	0.0063
49	36	14.08472	0.0057

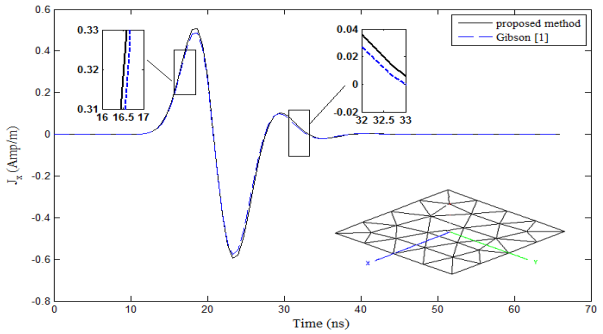

Fig. 5. The *x*-directed induced surface current density at the center of the 1m × 1m square PEC plate.

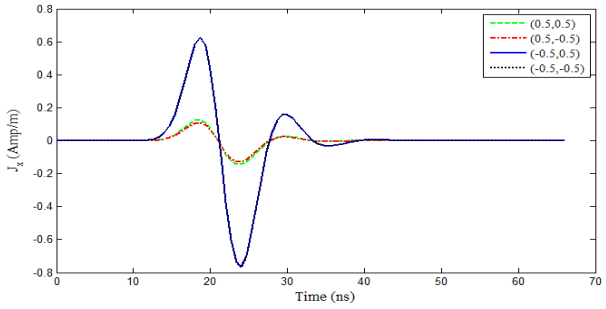

Fig. 6. The *x*-directed induced surface current density at the corners of the 1m × 1m square PEC plate.

As a second example, the *x*-directed current density at the center of an equilateral triangle by means of two methods is shown in Fig. 7. The triangle is subdivided to 29 triangular patches with 35 unknowns. Figure 8 shows the current density at two *x*-axis symmetric points A and B in corners of the triangle.

In the third example, a unit circle that subdivided to 94 triangular patches with 129 unknowns has been considered. Figure 9 shows the *x*-component of the induced current density at the center of this circle by means of two methods. In Fig. 10, the *x*-directed induced current density at two symmetry points on central cross section of the circle is shown.

As the last consideration, we obtain the *x*-directed induced surface current density at point (0,0,0) of a pie shaped plate. The geometry consists of an equilateral triangular plate 1 m on a side joined to a semicircular disk with a 1 m diameter. The plate lies in the *xy* plane with the "center" of the disk located at the origin. The triangular portion is divided into 23 triangles. Also, the disk portion is divided into 16 triangular patches resulting in a total of 39 patches with 74 unknowns. Figure 11 shows the *x*-component of the induced current density for both the proposed method and the Gibson method [1].

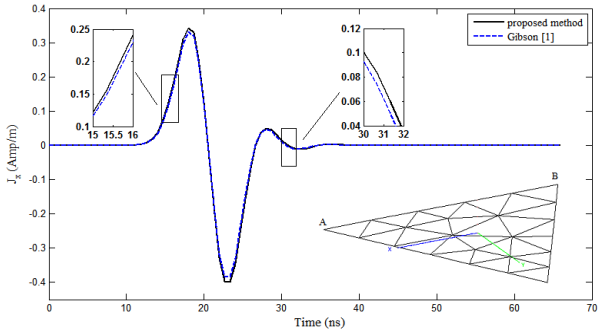

Fig. 7. The *x*-directed induced surface current density at the center of a unique equilateral triangle.

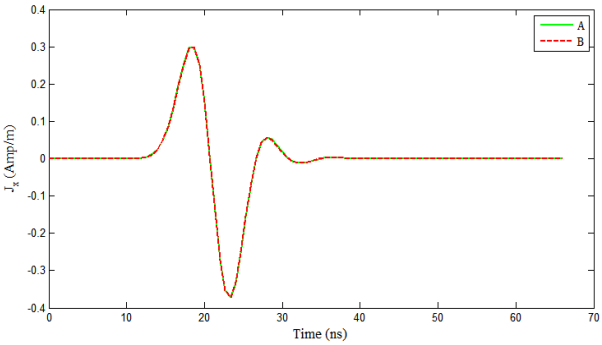

Fig. 8. The current density at two *x*-axis symmetric points A and B in the corners of the triangle.

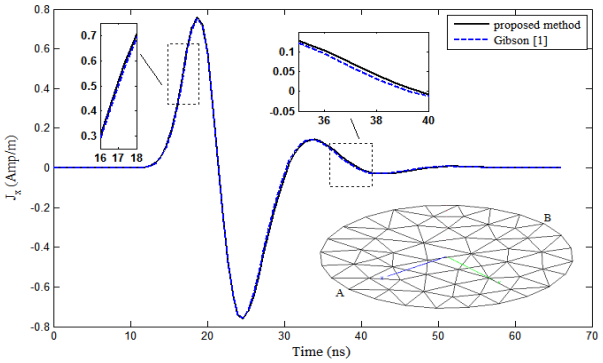

Fig. 9. The x-directed induced surface current density at the center of a unit circle.

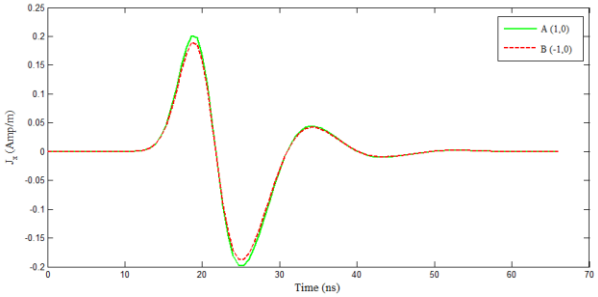

Fig.10. The *x*-directed induced surface current density at two symmetry points on central cross section of the circle.

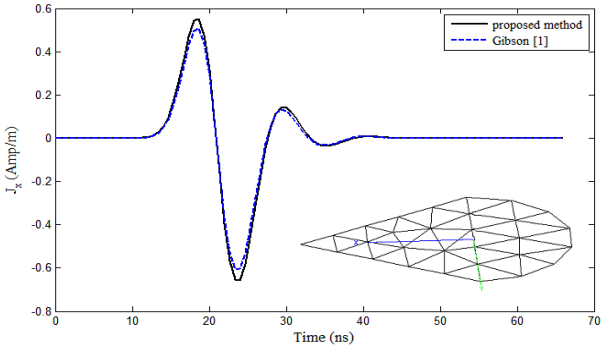

Fig. 11. The *x*-directed induced surface current density at the center of a pie shape.

Relative error between two implemented methods is calculated and shown in Table 2. It is observed that the relative error is smaller than 0.1 percent for all the cases, that means the proposed method is sufficiently accurate. To approve the outstanding property of the presented method, the computation time is reported in Table 3. Note that, the proposed method is about three times faster than the other. The computer used in this comparison has an Intel Core 2 CPU 2.13 GHz processor and 2 GB of RAM.

Table 2: Relative error between the Gibson Method [1] and the proposed method (in percent)

Object	Relative Error
Unit square	0.0063
Triangle	0.0021
Unit circle	0.0047
Pie shape	0.0263

Table 3: Comparison of the computation time between two methods (time in seconds)

Object	Proposed Method	The Gibson Method [1]
Unit square	8.67100	33.30909
Triangle	3.92005	12.97828
Unit circle	38.67338	159.68715
Pie shape	6.85649	24.96783

IV. CONCLUSION

In this work, we presented a computationally efficient method to obtain the solution to the potential integrals of time domain integral equations for the PEC surfaces in free space. This method by selecting some points in the source and observation patches in the MoM context, numerically calculate the potential integrals and does not encounter the singularity of self-terms. This method can be applied for the integral equation formulation of scattering problems dealing with singularity of 1/R. We used the proposed method for triangular basis functions while this method can be used for each arbitrary shapes of basis functions.

In addition, the proposed method can be used to analyze planar PEC structures in multilayered media for both frequency and time domains. It is expected that results of these studies will be reported in the near future.

REFERENCES

[1] W. C. Gibson, *The Method of Moments in Electromagnetics*. CRC Press, 2014.

[2] G. Carvajal, D. Duque, and A. Zozaya, "RCS estimation of 3D metallic targets using the moment method and Rao-Wilton-Glisson basis functions," *ACES Journal-Applied Computational Electromagnetics Society*, vol. 24, pp. 487, 2009.

[3] G. Manara, A. Monorchio, and R. Reggiannini, "A space-time discretization criterion for a stable time-marching solution of the electric field integral equation," *IEEE Transactions on Antennas and Propagation*, vol. 45, pp. 527-532, 1997.

[4] Q.-Q. Wang, C. Yan, Y.-F. Shi, D.-Z. Ding, and R.-S. Chen, "Transient analysis of electromagnetic scattering using marching-on-in-order time-domain integral equation method with curvilinear RWG basis functions," *ACES Journal-Applied Computational Electromagnetics Society*, vol. 26, pp. 429-436, 2011.

[5] R. F. Harrington and J. L. Harrington, *Field Computation by Moment Methods*. Oxford University Press, 1996.

[6] I. Hanninen, M. Taskinen, and J. Sarvas, "Singularity subtraction integral formulae for surface integral equations with RWG, rooftop and hybrid basis functions," *Progress In Electromagnetics Research*, vol. 63, pp. 243-278, 2006.

[7] M. A. Khayat and D. R. Wilton, "Numerical evaluation of singular and near-singular potential Integrals," *IEEE Transactions on Antennas and Propagation*, vol. 53, pp. 3180-3190, 2005.

[8] M. G. Duffy, "Quadrature over a pyramid or cube of integrands with a singularity at a vertex," *SIAM Journal on Numerical Analysis*, vol. 19, pp. 1260-1262, 1982.

[9] A. Azari, Z. H. Firouzeh, and A. Zeidaabadi-Nezhad, "A new efficient technique for transient scattering of conducting cylinders illuminated by a TM-polarized plane wave," *IEEE Antennas and Wireless Propagation Letters*, vol. 13, pp. 1421-1424, 2014.

[10] Z.-J. Qiu, J.-D. Xu, G. Wei, and X.-Y. Hou, "An improved time domain finite element-boundary integral scheme for electromagnetic scattering from 3-D objects," *Progress In Electromagnetics Research*, vol. 75, pp. 119-135, 2007.

[11] M. J. Bluck, M. D. Pocock, and S. P. Walker, "An accurate method for the calculation of singular integrals arising in time-domain integral equation analysis of electromagnetic scattering," *IEEE Transactions on Antennas and Propagation*, vol. 45, pp. 1793-1798, 1997.

[12] A. Herschlein, J. V. Hagen, and W. Wiesbeck, "Methods for the evaluation of regular, weakly singular and strongly singular surface reaction integrals arising in method of moments," *DTIC Document*, 2002.

[13] A. Tzoulis and T. F. Eibert, "Review of singular potential integrals for method of moments solutions of surface integral equations," *Advances in Radio Science*, vol. 2, pp. 93-99, 2005.

[14] S. N. Makarov, *Antenna and EM Modeling with Matlab*. New York, Wiley-Interscience, 2002.

[15] S. M. Rao, *Time Domain Electromagnetics*. Academic Press, 1999.

[16] S. Rao, D. Wilton, and A. Glisson, "Electromagnetic scattering by surfaces of arbitrary shape," *IEEE Transactions on Antennas and Propagation*, vol. 30, pp. 409-418, 1982.